Carbohydrate Polymer Technologies and Applications 8 (2024) 100610

Contents lists available at ScienceDirect

Carbohydrate Polymer Technologies and Applications

journal homepage: www.sciencedirect.com/journal/carbohydrate-polymer-technologies-and-applications

Chitosan-based multimodal polymeric nanoparticles targeting pancreatic β-cells

Lorenzo Rossi [a,1], Cataldo Pignatelli [a,b,1], Krisztina Kerekes [c,1], Francesca Cadamuro [a], András Dinnyés [d,e], Felix Lindheimer [f], Jochen Seissler [g], Magdalena Lindner [f], Sibylle Ziegler [f,h], Peter Bartenstein [f], Yi Qiu [i], Judit Kovács-Kocsi [c], Zoltán Körhegyi [c], Magdolna Bodnár [c], Erika Fazekas [c], Eszter Prépost [c], Francesco Nicotra [a], Laura Russo [a,j,*]

[a] Università degli Studi di Milano-Bicocca, School of Medicine and Surgery, Monza, Italy
[b] San Raffaele Diabetes Research Institute, IRCCS San Raffaele Scientific Institute, Milan, Italy
[c] BBS Nanotechnology, Debrecen, Hungary
[d] Biotalentum Ltd, Gödöllő, Aulich Lajos utca 26 2100 Hungary
[e] Hungarian University of Agriculture and Life Sciences, Institute of Physiology and Animal Nutrition, Department of Physiology and Animal Health, Gödöllő 2100 Hungary
[f] Department of Nuclear Medicine, University Hospital LMU Munich, Munich, Germany
[g] Medizinische Klinik und Poliklinik IV, Diabetes Zentrum - Campus Innenstadt, Klinikum der Ludwig-Maximilians-Universität, München, Germany
[h] Department of Nuclear Medicine, Hannover Medical School, Hannover, Germany
[i] iThera Medical GmbH, Zielstattstraße 13 81379 Munich, Germany
[j] Fondazione IRCCS San Gerardo dei Tintori, Monza, Italy

ARTICLE INFO

Keywords:
Chitosan
GLP-1R targeting
Beta-cell targeting
Exendin-4
Multimodal imaging
Diagnostic nanoparticles
Pancreatic islets

ABSTRACT

Multimodal in vivo imaging of pancreatic islets might improve monitoring of endocrine grafts upon implantation, helping clinical validation of new regenerative therapies based on the replacement of β-cells in type 1 diabetes affected patients. Herein, the generation of chitosan-based multimodal diagnostic nanoparticles (NPs) able to target β-cells is described. The NPs, composed of chitosan (CH) and γ-poly-glutamic-acid (γ-PGA) with different "clickable" functional groups were chemoselectively decorated at the surface with Exendin-4 (Ex4), a ligand of glucagon-like peptide 1 (GLP-1) β-cell receptors, and with a DOTA containing linker, to chelate diagnostic radioisotopes. Furthermore, the NPs were conjugated with IRDye®800CW for multispectral optoacoustic tomography (MSOT). The affinity of Ex4 decorated NPs towards GLP-1R was confirmed by competitive flow cytometry tests. The detectability of the NPs labeled with IRDye®800CW and Ex4 in MSOT experiments was demonstrated. In vivo biodistribution of Ex4 decorated NPs labelled with Ga-68 was studied with positron emission tomography (PET) experiments in mice. Specific binding to GLP-1 receptor expressing tissue was demonstrated in autoradiography experiments, showing potential of the multimodal NPs for specifically targeting β-cells.

Introduction

Multimodal *in vivo* imaging of pancreatic β-cells to monitor their presence and activity is object of great interest in the therapies for type 1 diabetes (Montet et al., 2013; Wei et al., 2019). The chance of following them in vivo is advantageous for the validation of novel strategies aimed at replacing the β-cells mass, as it can provide data to evaluate the health state of the endocrine engraft and to predict the outcome of the islet transplantation (Li et al., 2016). In fact, to date, to follow the evolution of islets transplantation, glucose level (Yu et al., 2020) and C-peptide (Maddaloni et al., 2022) monitoring is mostly used, an approach not very efficient (Caldara et al., 2023). The development of efficient tools able to target the pancreatic β-cells and detect their viability can bring benefits in the promising field of the β-cells replacement (Caldara et al., 2023; Murakami et al., 2021).

Several approaches have been experimented for in vivo detection of

* Corresponding author at: University of Milano – Bicocca, School of Medicine and Surgery, Via Follereau 3 20854 Vedano al Lambro (MB), Italy.
E-mail address: laura.russo@unimib.it (L. Russo).
[1] Lorenzo Rossi, Cataldo Pignatelli and Krisztina Keres equally contributed.

https://doi.org/10.1016/j.carpta.2024.100610

Available online 19 November 2024

β-cells. To follow transplanted β-cells in TD1 animal models, pre-transplanted pancreatic islet have been labeled with magnetic iron oxide nanoparticles (MNPs)(Jirák et al., 2004; Oishi et al., 2013; Zacharovová et al., 2012). In this way, the whole islet was labeled due to uptake of MNPs by islet macrophages (Berkova et al., 2008). However, this strategy resulted in a partial impairing of β-cells activity (Jirák et al., 2004; Kim et al., 2013) and, more importantly, did not allow to discern non-functional β-cells from functional ones. Thus, the research addressed to detect functional β-cells by targeting GLP-1R (Christ et al., 2009; Drucker, 2003; Jansen et al., 2019; Wang et al., 2014; Wild et al., 2016; Wild et al., 2010; Zhang et al., 2013). GLP-1R is able to trigger insulin secretion by β-cells, through the interaction with GLP-1(Ahren, 2009; Drucker, 2003). GLP-1R is highly expressed on β-cell membranes and even more on insulinoma cells (Körner et al., 2012; Lebastchi & Herold, 2012). Exendin-4 (Ex4) is a 39-peptide agonist of GLP-1R able to promote insulin secretion and approved by FDA to treat diabetes. It has been recently used also for diagnostic purposes conjugated to MNPs or labelled with SPECT and PET tracers (Jansen et al., 2019; Wang et al., 2014; Zhang et al., 2013). Several labelled Ex4 have been already assessed in preclinical and clinical studies, (Lindheimer et al., 2023; Reiner et al., 2011; Sidrak et al., 2023) which, notwithstanding, showed an important uptake by kidneys(Jansen et al., 2019). This entails possible toxic effects on kidneys and a difficult pancreatic β-cell imaging caused by overlapping signals from kidneys(Jansen et al., 2019; Wild et al., 2016, 2010). Considering the current limitations in β-cells imaging, stable diagnostic system that allow to detect β-cells with multimodal systems without affect their availability and reducing also the toxic effect on kidneys are needed. Here we describe the development of new diagnostic chitosan-poly-γ-glutamic acid nanoparticles (CH-γ-PGA NPs) able to target β-cell. These NPs were surface-functionalized by click chemistry with Ex4 to target GLP-1R, and with DOTA chelator for PET imaging, with potential applications in SPECT or MRI. Additionally, the NPs contained also a near-IR dye (IRDye® 800CW) for optoacoustic detection (MSOT). Our hypothesis is that these nanoparticles tools will enhance targeting of pancreatic β-cells and enable non-invasive detection of their viability in patients.

Materials and methods

Chemical and materials

Chitosan (CH; degree of deacetylation = 75–85 %, Mw = 50–190 kDa) was purchased from Sigma-Aldrich Co., Hungary and further deacetylated by treatment of chitosan with 10 M NaOH for 4 h at 100 °C, filtered and dialyzed against distilled water. The solution was lyophilized to obtain a white chitosan powder. Poly-γ-glutamic acid (γ-PGA, Mw = 100 kDa) was purchased from Shandong Freda Biotechnology Co., Ltd., China, and was used without further purification. N-hydroxy-succinimide (NHS), 1-Ethyl-3-(3-dimethylaminopropyl)-carbodiimide (EDC), 2-(aminomethyl)-furan (FA), azido-dPEG®$_4$-carboxylic acid (N_3-PEG_4- carboxylic acid), phosphate buffer phosphate (PBS), 2-(N-Morpholino)-ethane-sulfonic acid hydrate (MES), deuterium oxide (D_2O) were purchased from Sigma-Aldrich (USA). Tetraxetan-NHS (DOTA-NHS), and tetraxetan-bicyclo[6.1.0]non-4-yne (DOTA-BCN) were purchased from CheMatech (France). Exendin-4 (Ex4) and exendin-4-PEG_4-maleimide (Ex4-PEG_4_Mal) were purchased from Proteo-Genix (USA). IRDye® 800CW NHS ester was obtained from Li-Cor Biosciences.

^{1}H NMR

^{1}H Nuclear Magnetic Resonance (NMR) analysis was performed with a Varian 400 MHz Mercury instrument; chemical shifts were adjusted respect to deuterium oxide peak (4.790 ppm). The pulse angle was 90° and the relaxion delay 2 s, while the number of scans was 1000. Infrared analysis of polymers was performed with a PerkinElmer Spectrum 100 equipped with a Universal ATR (UATR). All the spectra were acquired in a spectral range from 4000 to 650 cm^{-1}, with a scanning resolution of 2 cm^{-1}, accumulating 30 scans each.

SEC—HPLC

Size exclusion chromatography analysis of polymers and NPs was carried out with a Waters e2695 Separations Module (Waters Co., Milford, MA, USA) equipped with a PDA detector (Waters 2998 Photodiode Array Detector) using a BioSec5 300 Å column (Agilent, 7.8 × 300 mm,5 μm) and it's guard column (Agilent, 7.8 × 50 mm, 5 μm). The flow rate was set to 1 mL/min using isocratic elution and the column was maintained at 30 °C. The eluent was 150 mM sodium phosphate buffer.

Polymers functionalization

γ-PGA-FA1 and γ-PGA-FA2

PGA was functionalized as previously reported in Rossi et al. (2022a). Briefly, to a solution of γ -PGA (100 mg, 0.69 mmol) in MES buffer 0.1 M pH = 5.5, NHS/EDC (1eq. each) were added as powder and the solution was stirred for 30 min a room temperature. Successively, FA (0.5 eq.) was added dropwise, and the solution was stirred overnight at room temperature and then was dialyzed with a tube having a MWCO of 14 kDa for 2 days, firstly against NaCl 0.1 M then with MilliQ water. Freeze-drying provided γ-PGA-FA-1 as a powder (74 mg, 73 % yield).

The same protocol, employing 2 eq. of NHS /EDC, and 2 eq of FA provided γ -PGA-FA-2 (77 mg, 70 % yield).

CH—N_3

N_3-PEG_4-carboxylic acid (37.8 mg, 0.13 mmol) was dissolved in 3 mL of MES buffer solution 0.1 M pH = 5.5; NHS/EDC (0.5 eq. each) were added as powder, the final solution was stirred for 45min. and then added dropwise to a CH solution (100 mg, 0.52 mmol) in MES buffer 0.1 M pH = 5.5 (7 mL). After 6 h, the solution was adjusted to pH 5.5, and NHS/EDC (0.5 eq. each) were added. The final solution was stirred overnight at room temperature and then dialyzed with a tube having a MWCO of 14 kDa for 2 days, firstly against NaCl 0.1 M then with MilliQ water. Freeze-drying provided CH—N_3 as powder (95 mg, 70 %). The product was characterized by ^{1}H NMR and FTIR analysis (1.2 Supplementary)

The functionalization grade of CH—N_3 was calculated by integrating the ^{1}H NMR peak of the -CH_2–N_3 protons at 3.33 ppm with respect to proton of –CH—NHC═O- at 2.92 ppm of chitosan (Fig. 1SI).

CH-IRDye

Chitosan lyophilized powder was solubilized in MilliQ water, and then adjusted to pH 6. The chitosan solution (V = 10 ml, c = 3 mg/mL) was mixed with IRDye® 800CW (V = 50 μL, c = 10 mg/mL in DMSO), and the reaction mixture was stirred in dark at room temperature for 24 h Fluorescently labeled chitosan (CH-IRDye) was purified on a hollow fiber filtration product (mPES, 10 kDa; Spectrum Laboratories Inc, CA, USA) against distilled water and acetate buffer solution (pH = 4). The purified product was lyophilized.

NPs formulation

Nanoparticles were formed by cross-linking of modified macromolecules after self-assembly.(Körhegyi et al., 2019) Briefly, aqueous solutions of modified γ-PGA (c = 0.3 mg/mL) and modified CH macromolecules (c = 0.3 mg/mL) were mixed at ratio of 3:1 at room temperature using intensive stirring for 30 min. To produce cross-linked nanoparticles, dropwise addition of water-soluble carbodiimide solution was performed and the reaction mixture was stirred at 4 °C for 4 h, then at room temperature for 20 h The solution containing cross-linked nanoparticles was purified from the unreacted macromolecules and carbodiimide by size exclusion chromatography (SEC) (qEV columns

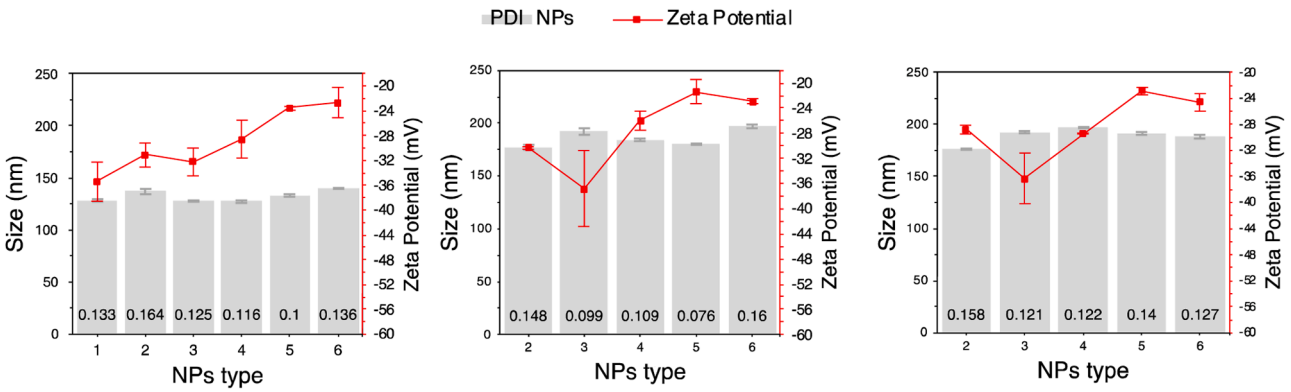

Fig. 1. NPs size and zeta potential in different media, before and after the functionalization. (A) Unfunctionalized NPs in MilliQ water. (B) Unfunctionalized NPs in PBS, pH 7.4. (C) Ex4 and DOTA functionalized NPs in PBS, pH 7.4.

with 70 nm exclusion limit, Izon, UK). The elution was performed with PBS, the separation was checked by HPLC-SEC system.

Surface functionalization of NPs with Ex4 and DOTA

A stock solution of Ex4-PEG_4-Mal, with a concentration of 1.4 mM, was prepared in PBS 0.01 M pH = 7.4. For the conjugation, 1 eq. of Ex4-PEG_4-Mal with respect to γ-PGA-FA functionalization was considered. More precisely, to calculate the amount of Ex4-PEG_4-Mal, the starting mass of γ-PGA-FAs used to formulate NPs was taken in account. So, a proper volume of Ex4-PEG_4-Mal stock solution was added dropwise to each kind of NPs, which were previously put in PBS 0.01 M pH = 7.4. Therefore, 1.4 μmol (6.3 mg) were dropwise added to type 1, 2, 3 and 4 NPs solutions, while 3.5 μmol (16 mg) were added to type 5 and 6 NPs solutions. Similarly, a 1.6 mM DOTA-BCN stock solution was prepared in PBS 0.01 M pH = 7.4. 1 mL of this solution was added to each NP types in order to have 1 eq. of DOTA-BCN respect to the azide functionalization, considering the starting mass of CH—N_3 used to formulate the NPs. All the solutions were stirred for 18 h at 4 °C. Addition of Ex4-PEG_4-Mal or DOTA-BCN to solution having NP without one of the functional groups or both (furan or azide groups), allowed to assess the absence of aspecific adsorption onto NPs surface.

The functionalized NPs were purified bySEC (qEV columns with 70 nm exclusion limit, Izon, UK). The elution was performed with PBS, the separation was checked by HPLC-SEC system.

NPs size and concentration measurements

All NPs, before and after functionalization, were characterized with dynamic light scattering (DLS), and nanoparticle tracking analysis (NTA).

The size was measured in different solvents accordingly to the stages of the preparation (water, PBS, labelling buffer) and the planned in vivo applications (plasma/serum of different species (mouse, pig and human). Plasma and serum for the ZetaSizer measurements were diluted two times by PBS to decrease the noise of the natural background of these physiologic substances.

Hydrodynamic size, size distribution, electrophoretic mobility, and Zeta potential of particles were measured using DLS technique with ZetaSizer Nano ZS (Malvern, UK)). Samples were analysed at 25 °C with a scattering angle of 173° and a 633 nm HeNe laser based on a material refractive index (RI) of 1.59, a dispersant refractive index of 1.330. The mean hydrodynamic diameter was calculated from the autocorrelation function of the intensity of light scattered from the particles. Each sample was measured three times, and the average data was calculated.

Electrophoretic mobility and Zeta Potential of the NPs were measured in automatic mode with minimum runs of 10, in folded capillary cells. Each sample was measured three times, and the average data was calculated. NTA was performed with NanoSight NS300 (Malvern, UK) to determine the exact concentration (particle number/mL), hydrodynamic size, size distribution. The examined polymer concentration for all NPs types was 1 μg/mL in PBS pH 7.4. Five acquisitions of 1 min were performed at 25 °C with a Blue488b laser, a camera level of 11 and a slider gain of 146, and analyzed by the in-build NanoSight Software NTA 3.1 Build 3.1.46 with a detection threshold of 2.

Quantification of Ex4 molecules on the surface of NPs

We examine the presence of Exendin-4 molecules on the surface of NPs based on recognition by Alexa Fluor 488 conjugated polyclonal anti-Exendin-4 antibody (Bioss Inc).

The binding of the antibody to the NPs was detected by ZetaView TWIN instrument (Particle Metrix, Germany). The solution of labelled NPs was purified from the unbound antibodies by SEC (qEV columns with 70 nm exclusion limit, Izon, UK) to eliminate the background of the fluorescence measurement and allow high sensitivity detection.

The number of binding antibodies to the NPs was determined in a competitive flow cytometric assay. In this test the Ex4-conjugated NPs should compete with Ex4-coated beads (avidin-coated beads (Spherotech Inc) conjugated with Exendine4-biotin (AnaSpec Inc)) for the Alexa 488 conjugated anti-Ex4 antibodies and the antibody consumption of the NPs was assessed based on the fluorescence of the beads measured by flow cytometer. The calibration of the assay with known amounts of free Ex4 molecules allowed the determination of the exact number of Ex4 molecules/NP.

Affinity test (cell-based assay)

The binding ability of Ex4-NPs to GLP-1R was examined in competitive flow cytometric assay. GLP-1R positive Beta-TC-6 cells (ATCC) were incubated with 10 nM fluorescein-labeled Ex-4 (Eurogentec) alone or together with our constructs and the binding ability of a construct was calculated based on the inhibition of the fluorescent Ex-4 derived sign. The fluorescence of the cells was measured by flow cytometer (BD FACSCalibur). Flowing Software was used for data evaluation. The relative affinities were defined as the ratio of concentrations of Ex4-NP sample required to displace 50 % of fluorescent Ex-4 bound to the GLP-1R of beta cells:

$$\textit{relative affinity } (RA) = \frac{IC_{50}(Ex4 - PEG - maleimide)}{IC_{50}(Ex4 - NPs)}$$

Transmission Electron Microscopy (TEM)

Transmission electron microscopy images were acquired using a JEM-2100 Plus electron microscope (Jeol, Japan). The nanoparticles

were adsorbed on carbon ultrathin support film on grids, and then washed three times with MilliQ water to remove the PBS salts. Successively, they were stained with uranyl acetate 1 %.

Detection of NPs-IRDye with MSOT

NP samples were filled inside clear plastic straws of 3 mm diameter. Estimated concentrations for the NPs were: NP 7.14×10^{11} mL^{-1}, NP-IR 1.69×10^{11} mL^{-1}, Ex4-NP-IR $1.681.69 \times 10^{11}$ mL^{-1}. The straws were inserted into a scattering non-absorbing phantom made of 1.8 % agarose and 1 % intralipid. The phantom with samples were scanned with a small animal scanner MSOT inVision 256-TF (iThera Medical, Munich, Germany). Signal was acquired at every 5 nm from 680 nm to 980 nm. For each wavelength, 3 frames were averaged to increase signal-to-noise ratio. The images were reconstructed with backprojection algorithm using viewMSOT 4.0 software. A region of interest (ROI) was draw around the straw in the cross-sectional image. Mean signal intensity inside the ROI at each wavelength was plotted to obtain the optoacoustic spectra of the NP samples.

In vitro testing

Cytotoxicity test

The possible toxicity effect of polymer and NP samples on Beta-TC-6 cells (ATCC) were tested by CytoTox-Glo Cytotoxicity Assay (Promega) according to the manufacturer's instructions. The ratio of dead/total cells in the cell cultures were determined after 3, 24 and 48 h treatment. The polymers and NPs were used at end concentration equivalent of plasma concentration applied *in vivo*. The assay was performed in 384 well white, tissue culture plates, the luminescence was measured by Synergy H1 microplate reader (BioTek).

In vitro complement activity test

The possible complement activating effect of polymers and NP samples was examinated *in vitro* by MicroVue SC5b 9 Plus Enzyme Immunoassay (Quidel) according to the manufacturer's instructions. This assay measures the concentration of TCC thereby giving an indication of the status of the terminal complement pathway in the sample. The polymers and NPs were used at end concentration equivalent of plasma concentration applied *in vivo*. Normal human serum was used as complement resource, the functional integrity of the complement system of the used serum was checked by positive controls suggested by the kit: zymosan as alternative pathway activator and immune complex as classical pathway activator were examined. The effect of differently functionalized NPs was compared to some clinically used nanomedicine (Caelyx and Abraxane).

Labeling of NPS-DOTA with GA-68

$Ga(III)Cl_3$ was eluted from a Ge/Ga-Generator (Eckert & ZieglerRadiopharma GmbH,Berlin, Germany) with 0.1 M HCl. The first 1.5 mL were discarded and 200 μL of the following 1 mL (containing up to 200 MBq) were added to a mixture of 100 μL of NaOAc buffer (0.5 M, pH 5) and 75 μL nanoparticle dilution (30–50 % NP in PBS). Final pH was between 4.2 and 4.5 to avoid aggregation of the nanoparticles. After labeling for 5 min at 85 °C and 900 rpm, the labeling yield was checked *via* iTLC in 0.5 M citrate buffer (pH 5). The mixture was added to a preconditioned (PBS) PD10 column. Fractionated elution with PBS (400 μL and three times 200 μL) was used to gain up to 80 MBq of highly purified nanoparticle solution (>97 %) in PBS (pH 7.4) which was then used for injection.

NPs biodistribution

In vivo PET imaging

Mice experiments were performed on a nanoScan-PET/CT (Mediso, Budapest, Hungary). After the mice (7 female) were anesthetized with isoflurane a CT-scan was conducted, followed by the application of about 5.0 ± 2.4 MBq of the NP solution injected into the tail vein with the beginning of the PET-scan (40 min). PET and CT Images were reconstructed using the nanoScan software and images were viewed and analysed with the PMOD image processing program (PMOD Technologies LLC, Zurich, Switzerland).

In vitro autoradiography

To study the binding properties of the ^{68}Ga labelled DOTA-NP-Ex4, 16 μm thick cryoslices of mouse muscle, pancreas and liver were prepared and placed on a microscope slide. These slides were preincubated with 200 mM Tris–HCl + 1 % BSA for 10 min. Afterwards 1 mL of a 2 nM ^{68}Ga labelled DOTA-NP-Ex4 solution in 200 nM Tris–HCl + 1 % BSA was added and incubated for 60 min, washed three times with 100 mL 200 mM Tris-Cl for 5 to 10 min and dried for 30 to 40 min at room temperature. The slides were placed on a photo plate and analyzed after 24 h with a CR-Reader (v.1.4.1, Elysia-raytest GmbH) and an Aida Image Analyzer software (v.4.50.010, Elysia-raytest GmbH). All mouse experiments were conducted according in compliance with the National Guidelines for Animal Protection, Germany, and with the approval of the regional animal committee (Regierung von Oberbayern, TVA AZ ROB-55.2Vet-2532.Vet_02–16–187).

Statistical analysis

All the experiments were conducted in at least three independent experiments. The results are presented as the mean ± (SD). Statistical analysis was performed by using a one-way ANOVA followed by Tukey's pairwise comparisons. The differences were considered significant at $p < 0.05$.

Results

CH and γ-PGA have been chosen as components for their capability to produce NP formulations with well-defined properties(Hajdu et al., 2008; Khalil et al., 2017; Lin et al., 2005). Additionally, both polymers are indeed suited for chemical modification in order to precisely design the final NPs(Khalil et al., 2017; Wang et al., 2020). In this work, the NPs must contain both Ex4 and DOTA at the surface to allow specific interaction with GLP-1R and chelation of the radioisotope for PET. The IRDye® 800CW, instead, can be attached to one of the NPs components, as its location at the surface is not necessary for MSOT detection. (Chang et al., 2019; Wang et al., 2023). The conjugation of Ex4 and DOTA at the NPs surface is a critical point, requiring experimental conditions preserving the NPs integrity and avoiding their contamination with side products, and therefore requires a so called click chemistry approach.

In our synthetic strategy we decided to use Ex4 functionalized at Lys-27 with a maleimide-containing linker, suitable for two alternative click chemistry conjugation approaches, the Diels-Alder with a dienophile such as furan (Cadamuro et al., 2020; Magli et al., 2020) or the Michael reaction with a thiol (Chang et al., 2019; Northrop et al., 2015). In our hand the first approach gave better results in terms of yield and reproducibility. γ-PGA was therefore functionalized with a furan group by reaction of with 2-(aminomethyl)-furan (FA), using N-hydroxy-succinimide (NHS) and 1-ethyl-3-(3-dimethylaminopropyl)-carbodiimide (EDC) as condensing agents, as previously reported(Rossi et al., 2022a). The surface functionalization with DOTA required a different and orthogonal click chemistry approach. We opted for the copper free strain promoted azide-alkyne cycloaddition(Agard et al., 2004), exploiting the commercially available tetraxetan-bicyclo[6.1.0] non-4-yne (DOTA-BCN) and functionalizing CH with an azido group. To this purpose the amino group of CH was reacted with N_3-PEG_4-carboxylic acid with NHS/EDC as condensing agents generating CH—N_3 as previously reported (Rossi et al., 2022b) (Scheme 1).

In both cases, the experimental conditions of condensations were strictly controlled in order to obtain an appropriate functionalization degree (D'este et al., 2014; Xu et al., 2019), high enough to grant proper

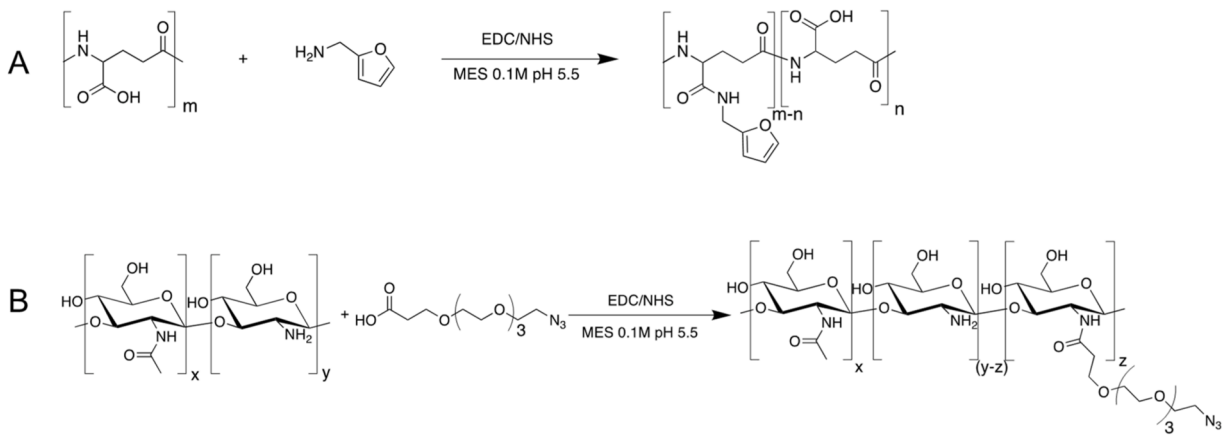

Scheme 1. Polymers functionalization. Chemical functionalization of A) γ-PGA with furfurylamine and B) chitosan with N_3-PEG_4-carboxylic acid.

Ex4 peptide and DOTA conjugation, but not so high as to not interfere with NPs assembling(Hajdu et al., 2008). The functionalized polymers were characterized by ^{1}HNMR and FTIR analysis (Supplementary Information and (Rossi et al., 2022b)).

Functionalization of γ-PGA (Scheme 1A) was performed and characterized as previously reported (Rossi et al., 2022b). Chitosan functionalization was performed by carbodiimide chemistry, using N_3-PEG_4-carboxylic acid (Scheme 1B). The ^{1}H NMR of CH—N_3 showed in Fig. 1SI in comparison with those of the starting materials, present the -CH_2—N_3 signal at 3.46 ppm and the PEG chains -CH_2—O- signal at 3.67 ppm. Additionally, at 2.4 ppm the signal of -CH_2—C = O protons indicate the amide bond formation. The functionalization grade of CH—N_3 was calculated by integrating the ^{1}H NMR peak of the -CH_2—N_3 protons at 3.46 ppm with respect to proton of –CH—NHC═O- at 3.07 ppm of chitosan.

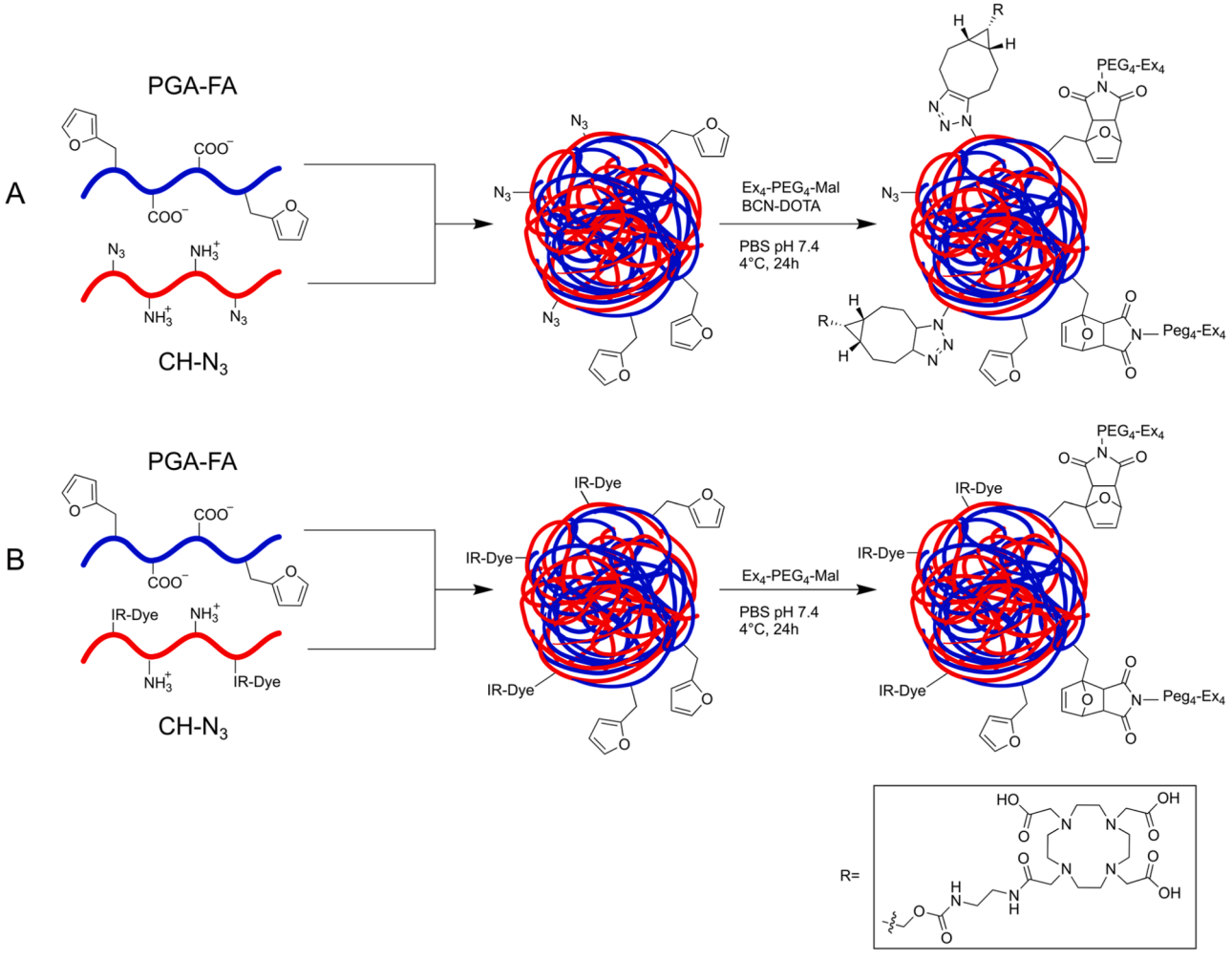

Scheme 2. Nanoparticle formulation and decoration. Formulation and decoration of: A) DOTA-NP-Ex4 and B) IR-NP-Ex4.

NPs formulation

Multiple types of NPs were prepared combining differently modified CH and γ -PGA by chemical crosslinking and ionic interactions. Both polymers are biocompatible and biodegradable and therefore suitable for biomedical applications fields(Antunes et al., 2011; Gao & Wu, 2022; Malhotra et al., 2013) including drug delivery systems (Castro et al., 2019, 2020; Chung et al., 2020; Hong et al., 2016) and regenerative medicine (Gao & Wu, 2022), imaging tools (Körhegyi et al., 2019)and biosensors. (Geng et al., 2013) The NPs properties can be easily tuned by varying the polymers ratio and molecular weight (Keresztessy et al., 2009). Considering the final application of our NPs for multimodal diagnostic imaging, we improved the stability of the NPs covalent crosslinking, in order to control the long-term stability of the formulations (Elsabahy et al., 2015; Kim et al., 2020). Briefly, self-assembled polyelectrolyte complexes were formulated by mixing the two polymers, exploiting the opposite charges displayed in solution, and cross-linked via carbodiimide chemistry. Thus, opaque aqueous colloidal systems containing either functionalized or not functionalized NPs were formed in accordance with the necessary expectations (Scheme 2). Not functionalized NPs (Type 1, CH-PGA) were prepared by cross-linking of self-assembled CH and γ -PGA polymers and used as reference. The azide-functionalized NPs (type 2, CH—N_3/PGA) were obtained combining γ-PGA with CH—N_3 and were employed as untargeted control particles. Two types of furan-functionalized NPs were prepared, starting from CH and γ-PGA-FA-1 and γ-PGA-FA-2, generating CH/PGA-FA-1 (type 3) and CH/PGA-FA-2 (type 5) with respectively a lower and a higher degree of furan derivatization. Finally, two types of multi-functionalized NPs were obtained, respectively from CH—N_3 and γ-PGA-FA-1 that generated CH—N_3/PGA-FA-1 (type 4), and from CH—N_3 and γ-PGA-FA-2, providing CH—N_3/PGA-FA-2 (type 6 NPs). Analogously, chitosan labeled with IRDye® 800CW (CH-IRDye) was combined with either γ-PGA or γ-PGA-FA-1 to generate IRDye containing NPs.

The dimensions of the different NPs are similar, all around 130 nm in water and around 180 nm in PBS at pH 7.4 (Fig. 1). The dimensions were not affected by the presence of furan and/or azide groups neither by higher nor lower functionalization of γ-PGA. Instead, according to the ζ-potential measurements (Fig. 1C), the surface charge resulted to be less negative when γ-PGA-FA functionalization increased, as expected for the decrease of the carboxylate groups that reacted with FA. The employment of CH—N_3 instead of CH also impacts on the resulting Z potential of NPs. This is particularly evident when comparing type 3 and 4 NPs, both composed by γ-PGA-FA-1. By contrast, no significant variation is detected between type 5 and 6 NPs, suggesting a different composition of the surface of NPs depending on the degree of functionalization of the employed γ -PGA-FA. Furthermore, IRDye labelled NPs show a similar trend, indicating a comparable influence between CH—N_3 and CH-IRDye on the resulting Z potential.

Surface functionalization of NPs with Ex4 and DOTA

The furan-functionalized NPs type 3 and type 5 were treated with exendin-4-PEG_4-maleimide (Ex4-PEG_4_Mal) in PBS 0.01 M pH = 7.4, resulting in the NPs functionalized at the surface with Ex4 with lower intensity (CH/PGA-Ex4 L) and higher intensity (CH/PGA-Ex4H). Similarly, the bis-functionalized NPs (type 4 and type 6) were submitted to one step double conjugation to both DOTA-BCN and Ex4-PEG_4_Mal, leading to NPs decorated at the surface with both DOTA and Ex4. Type 4 provided the NPs with less intense decoration with Ex4 (CH/PGA-Ex4L-DOTA), type 6 resulted in the higher Ex4 functionalization (CH/PGA-Ex4H-DOTA). The NPs functionalization reactions with Ex4 and DOTA were highly selective and did not alter NPs physical properties, as inferred by data (Fig. 1). In all the NPs samples (Table 1), after Ex4-PEG_4_Mal and/or DOTA-BCN conjugations, size did not significantly change, neither the ζ-potential (Fig. 1).

Table 1
Composition and characteristics of functionalized nanoparticles.

NPs type	NPs composition	CH/g-PGA ratio	NPs decoration	Average dimension (nm) in PBS pH 7.4	Measured Ex4/NP
1	CH/PGA	1:2	–	145	0
2	CH—N_3/PGA	1:2	DOTA	141	0
3	CH/PGA-FA-1	1:3	Ex4	188	310
4	CH—N_3/PGA-FA-1	1:3	DOTA and Ex4	182	350
5	CH/PGA-FA-2	1:3	Ex4	187	1220
6	CH—N_3/PGA-FA-2	1:3	DOTA and Ex4	178	1250

Quantification of Ex4 molecules on the surface of NPs

Ex4 conjugated NPs were treated with fluorescent A488 anti-Ex4 antibody and detected in both scattering and fluorescence modes by ZetaView® (Analytik Ltd); the measured concentration values were the same in the two modes indicating that all the NPs were labelled with the fluorescent antibody, and therefore contained Ex4 (Fig. 2 right). To prove the specificity of the labelling, Ex4-free NPs (type 2) treated in a same manner were used as negative control; in this case they were not detected in fluorescence mode but only in scattering mode (Fig. 2 left).

The measured number of Ex4 molecules on the surface of different constructs are reported in Table 2.

Affinity test and TEM analysis

The binding capability towards GLP-1R positive Beta-TC-6 cells (ATCC) of NPs decorated with Ex-4 (type 6, 1250 Ex4 molecules/NP) was investigated in competitive flow cytometry. Compared with the Ex4-PEG4-Mal molecule in which a single exendin unit is present, the affinity of our NPs towards GLP-1R was 35.7 times higher, indicating a cluster effect. The affinity towards GLP-1R of our NPs, stored in PBS at 4 °C, was measured for six months. We found that after 2 months the relative affinity started to decrease, presumably due to the degradation of the Ex-4 peptide. TEM analysis showed that the nanoparticles have spherical and regular shapes with good dispersibility in H_2O.

Detection of NPs-IRDye with MSOT

The feasibility of optoacoustic imaging exploiting the NPs functionalized with IRDye800CW was investigated with a MSOT scanner inVision 256-TF (iThera Medical, Munich, Germany) and compared to unfunctionalized NPs as well as NPs IR and Ex4 functionalization. Optoacoustic signal was acquired at every 5 nm from 680 nm to 980 nm. Fig. 3 shows optoacoustic signal of the nanoparticles at each acquired wavelength. The NPs labeled with IRDye800CW (NP-IR and Ex4-NP-IR) showed higher signal compared to unlabeled NPs, in particular in the wavelength range of 700–800nm. Noteworthy, also exendin contributes to the absorption increase, as shown by the signal of Ex4-NP-IR at 775 nm compared to that of NP-IR. These results indicate a good MSOT detectability of our diagnostic nanoparticles Ex4-NP-IR.

Stability tests

Type 2 and 6 nanoparticles stability was tested for their in vivo application in plasma and serum from different species to study potential undesirable increment in size or aggregation. In particular, plasma and serum of mouse, pig and human were employed for the test. In none of them aggregation was observed. In the case of pig and mouse serum and plasma, the size distribution of the nanoparticles showed increment up to 10 %. Furthermore, we tested the stability of nanoparticles type 2 and 6 and the not-decorated counterparts, stored as starting

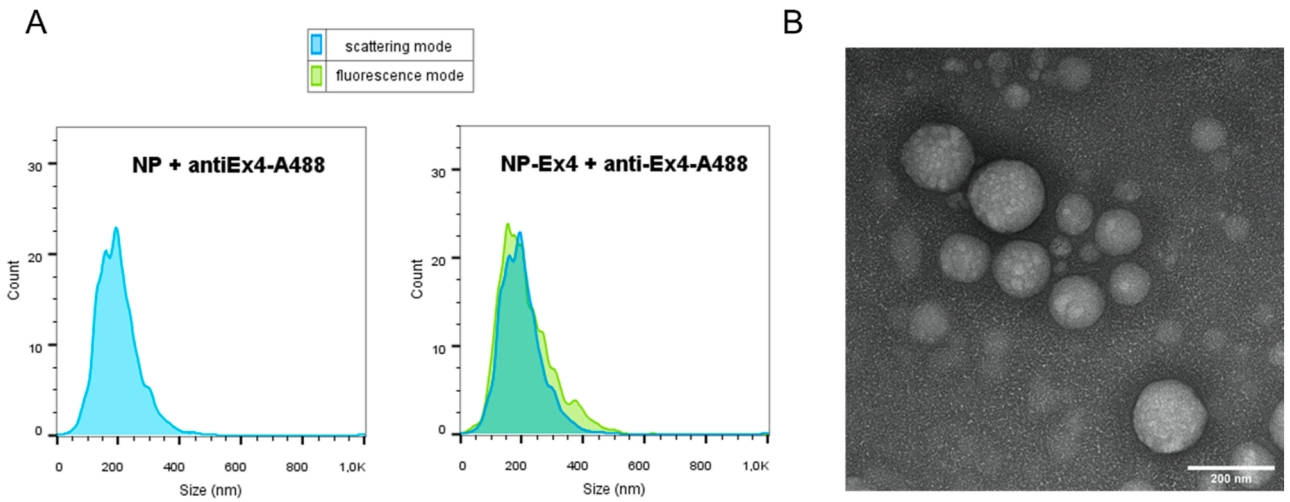

Fig. 2. A) Detection of the NPs in both scattering and fluorescent mode. Determination of type 6 nanoparticle decoration with Ex-4 by treatment with Alexa Fluor 488 labelled anti-Ex4 antibody. **B) TEM analysis**. TEM analysis of type 6 NPs functionalized with DOTA and Ex-4.

Table 2
Number of Ex4 molecules on the surface of NPs determined by Alexa Fluor 488 labelled anti-Ex4 antibody and relative affinity of NPs for GLP-1R measured on β-cells.

NPs composition	NPs type	measured Ex4/NP	relative affinity for GLP-1R
CH/PGA	1	0	0
CH—N_3/PGA	2	0	0
CH/PGA-FA-1	3	310	no data
CH—N_3/PGA-FA-1	4	350	no data
CH/PGA-FA-2	5	1220	no data
CH—N_3/PGA-FA-2	6	1250	35,7

nanoparticles. PGA-chitosan nanoparticles suspension in PBS at pH 7.4 and 4 °C resulted to be the optimal storage conditions. Concerning the dimensions, all the nanoparticles showed excellent stability up to 6 months (Fig. 4). We have followed the relative affinity of NPs to the GLP-1R with the cell-based assay for six months storage in PBS at 4 °C and we have found that after 2 months the relative affinity started to decrease presumably due to the degradation of conjugated Ex-4 polypeptide.

In vitro testing

All raw material used for preparation of CH/PGA NPs are biocompatible and FDA approved, however their possible cytotoxicity and complement activator effect were monitored. During the examined time there is no difference in relative number of dead cells in the treated and control cell populations (Fig. 5A). Based on the results the NPs and polymers have no toxic effect on the cell cultures.

The surface of nanoparticles may have possible activating effect on complement system, which is an integral component of innate immunity. We have checked for this potential source of risk before using our NPs *in vivo*. The MicroVue SC5b 9 Plus assay measures the amount of the Terminal Complement Complex (TCC, SC5b-9) generated by the assembly of C5 through C9 as a consequence of activation of the complement system by either the classical, lectin or alternative pathway. The effect of differently functionalized NPs was compared to some clinically used nanomedicine (Fig. 5B). Based on the results the NPs and polymers have no remarkable activator effect on the complement system that is very important point in case of an *in vivo* applied nanomaterials.

Labelling of NPS-DOTA with radioisotopes and evaluation of NPs biodistribution in vivo

In vivo PET experiments using ^{68}Ga labelled DOTA-NP-Ex4 Type 6

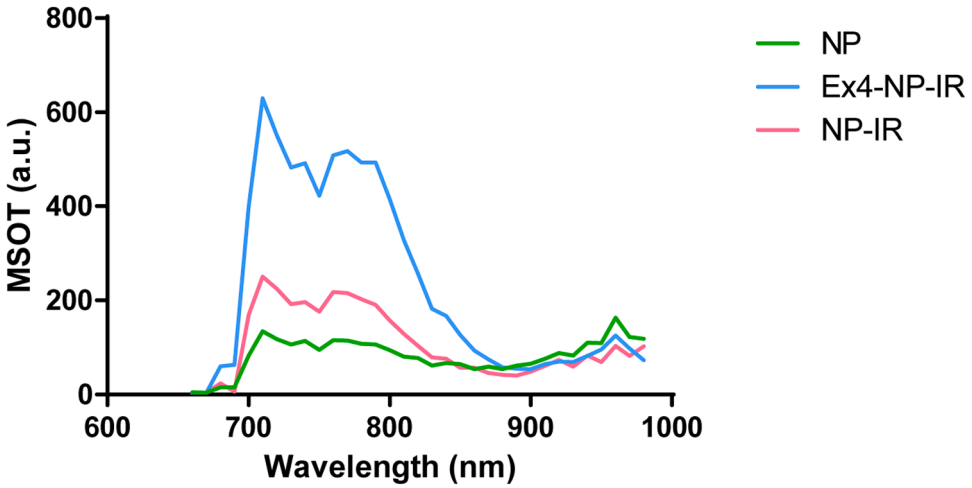

Fig. 3. Detection of NPs by MSOT. Optoacoustic signal from 680 to 980 nm of the 3 NPs was plotted.

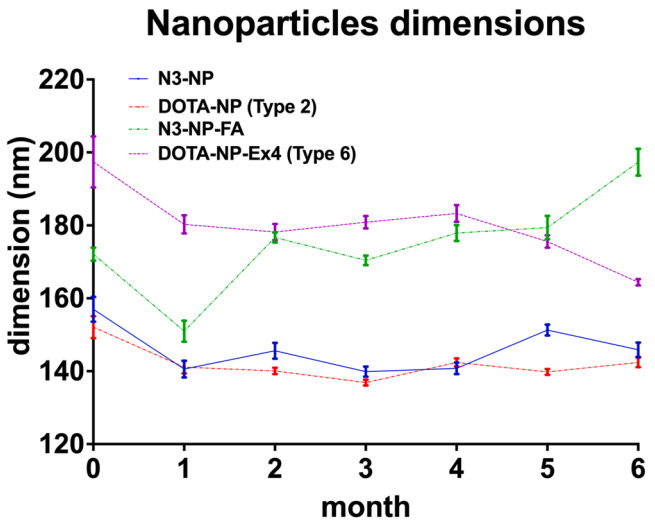

Fig. 4. Monitoring of nanoparticles dimensions over time. Nanoparticles dimensions monitored by NTA after up to 6 months of storage in PBS pH 7.4 at 4 °C.

were performed in mice to study their biodistribution in vivo. No side-effects after NP injection (6 MBq) were noticed. In mice ($n = 3$) a high uptake of the labeled NPs in the liver and much less in the lungs was observed, while general background levels (e.g. muscle) were very low (Fig. 6b). Since there is no GLP-1R expression in the liver, the PET signal reflects NP elimination in the liver. Potential specific binding in the pancreas of the mouse is not possible to determine because of the close proximity to the very high signal in the liver. To prove specific binding of the functionalized NPs, in vitro autoradiography on mouse tissue slices was performed. This showed a significant presence of ^{68}Ga labelled NPs functionalised with Ex4 in the pancreas, demonstrating the uptake and the capacity to accumulate by interacting with ß-cell GLP-1 receptors (Fig. 6c). This is the first example of polymeric biodegradable and biocompatible NPs able to target GLP-1, the other example of Ex4-functionalised NPs reported in the literature are magnetic-NPs (ref). Our Ex4-NPs show increased targeting ability to pancreas, with reduced liver and kidney accumulation, and allow multimodal detection (Vinet et al., 2015).

Conclusion

This work describes how to generate stable multi-functionalized nanoparticles suitable for multimodal diagnostic approaches. Combining chitosan and poly-γ-glutamic acid in both of which functional groups suitable for subsequent click chemistry reactions, nanoparticles of around 150–200 nm were obtained, suitable for surface decoration with ligands for targeting and multiple detecting agents. Specifically, the nanoparticles were functionalised at the surface with exendin-4, to target beta-cells, with IRDye800CW for MSOT optoacustic detection, with DOTA to chelate Ga-68 for PET. In vitro and in vivo (mice) experiments demonstrated the affinity of the nanoparticles for GLP-1-receptors and the diagnostic potential.

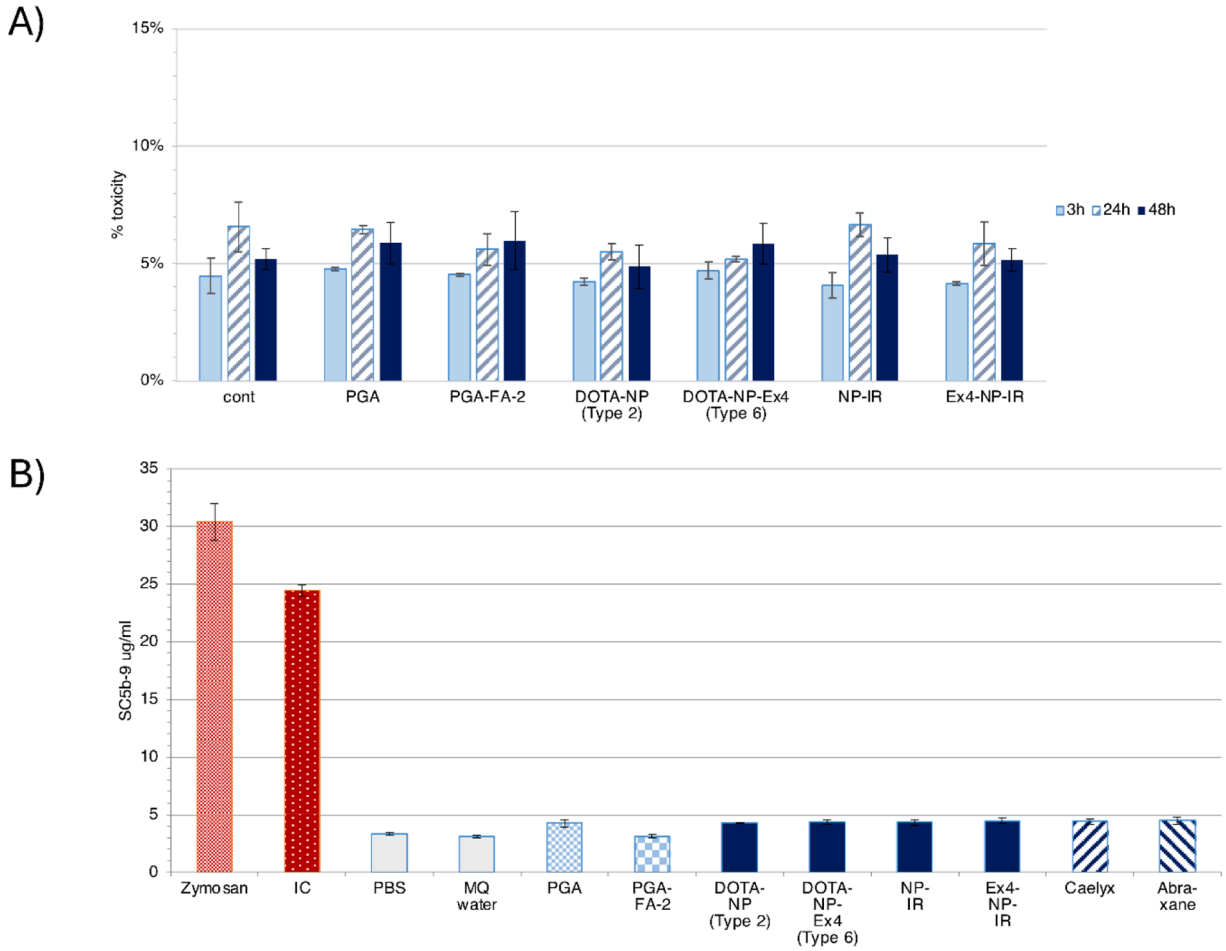

Fig. 5. Examination of possible cytotoxic (A) and complement activator (B) effect of polymer and NP samples.

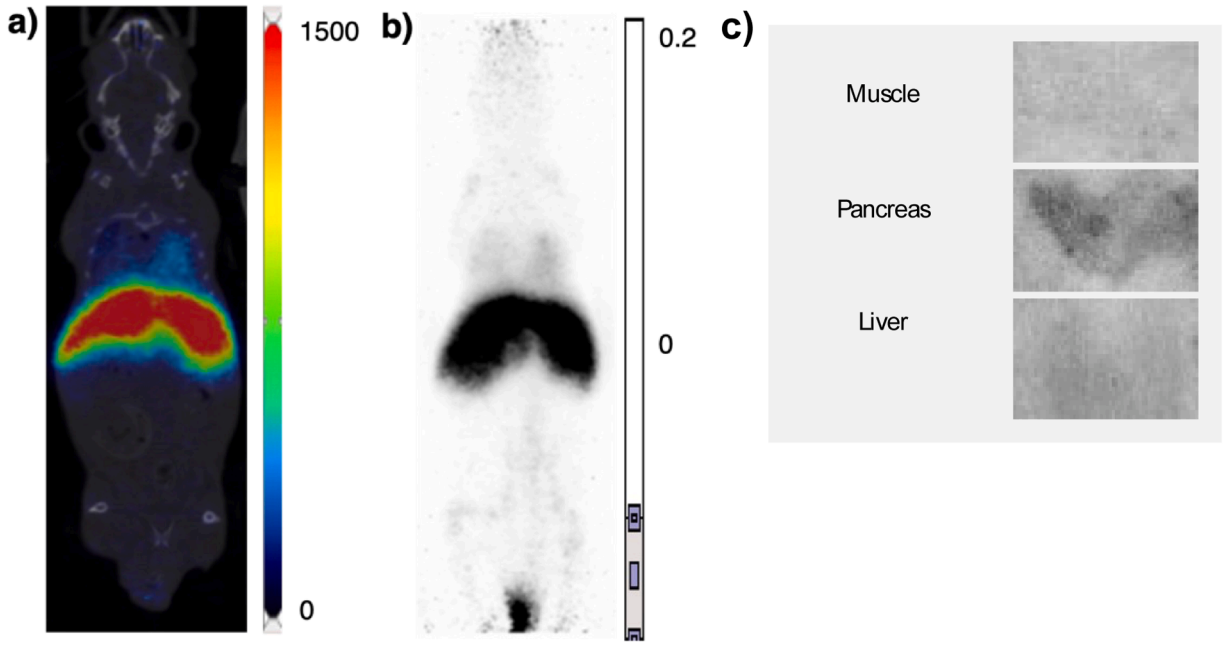

Fig. 6. In-vivo-biodistribution in the mouse model. a) coronal whole-body slice of ^{68}Ga-labelled DOTA-NP-Ex4 distribution in kBq/cc (30–40 min p.i.), overlayed to the corresponding CT slice and b) whole-body maximum intensity projection. c). In vitro autoradiography of ^{68}Ga labelled DOTA-NP-Ex4 on mouse muscle, pancreas and liver.

Ethics statement

The animal study was reviewed and approved by Regierung von Oberbayern (ROB-55.2–2532.Vet_02–22–65) and comply with the ARRIVE guidelines, EU Directive 2010/63/EU for animal experiments, and National Research Council's Guide for the Care and Use of Laboratory Animals.

CRediT authorship contribution statement

Lorenzo Rossi: Writing – original draft, Methodology, Investigation. **Cataldo Pignatelli:** Writing – original draft, Methodology, Investigation. **Krisztina Kerekes:** Methodology, Investigation. **Francesca Cadamuro:** Writing – original draft, Methodology, Investigation. **András Dinnyés:** Writing – review & editing, Project administration, Conceptualization. **Felix Lindheimer:** Methodology, Investigation. **Jochen Seissler:** Methodology, Investigation. **Magdalena Lindner:** Methodology, Investigation. **Sibylle Ziegler:** Methodology, Investigation. **Peter Bartenstein:** Methodology, Investigation. **Yi Qiu:** Methodology, Investigation. **Judit Kovács-Kocsi:** Methodology, Investigation. **Zoltán Körhegyi:** Methodology, Investigation. **Magdolna Bodnár:** Methodology, Investigation. **Erika Fazekas:** Methodology, Investigation. **Eszter Prépost:** Methodology, Investigation. **Francesco Nicotra:** Conceptualization. **Laura Russo:** Writing – review & editing, Supervision.

Declaration of competing interest

AD is founder and CEO of BioTalentum Ltd, and declare competing interest.

Acknowledgments

The research leading to these results has received funding from the European Union's Horizon 2020 research and innovation programme under grant agreement No 760986 (iNanoBIT "Integration of Nano- and Biotechnology for beta-cell and islet Transplantation").

Supplementary materials

Supplementary material associated with this article can be found, in the online version, at doi:10.1016/j.carpta.2024.100610.

Data availability

Data will be made available on request.

References

Agard, N. J., Prescher, J. A., & Bertozzi, C. R. (2004). A Strain-Promoted [3 + 2] Azide–alkyne cycloaddition for covalent modification of biomolecules in living systems. *Journal of the American Chemical Society, 126*(46), 15046–15047. https://doi.org/10.1021/ja044996f

Ahren, B. (2009). Islet G protein-coupled receptors as potential targets for treatment of type 2 diabetes. *Nature Reviews. Drug Discovery, 8*(5), 369–385.

Antunes, J. C., Pereira, C. L., Molinos, M., Ferreira-da-Silva, F., Dessì, M., Gloria, A., et al. (2011). Layer-by-layer self-assembly of chitosan and poly(γ-glutamic acid) into polyelectrolyte complexes. *Biomacromolecules, 12*(12), 4183–4195. https://doi.org/10.1021/bm2008235

Berkova, Z., Jirak, D., Zacharovova, K., Kriz, J., Lodererova, A., Girman, P., et al. (2008). Labeling of pancreatic islets with iron oxide nanoparticles for in vivo detection with magnetic resonance. *Transplantation, 85*(1), 155–159. https://doi.org/10.1097/01.tp.0000297247.08627.ff

Cadamuro, F., Russo, L., & Nicotra, F. (2020). Biomedical hydrogels fabricated using diels–alder crosslinking. *European Journal of Organic Chemistry*. https://doi.org/10.1002/ejoc.202001042

Caldara, R., Tomajer, V., Monti, P., Sordi, V., Citro, A., Chimienti, R., et al. (2023). Allo Beta Cell transplantation: Specific features, unanswered questions, and immunological challenge. *Frontiers in Immunology, 14*, Article 1323439. https://doi.org/10.3389/fimmu.2023.1323439

Castro, F., Pinto, M. L., Almeida, R., Pereira, F., Silva, A. M., Pereira, C. L., et al. (2019). Chitosan/poly(γ-glutamic acid) nanoparticles incorporating IFN-γ for immune response modulation in the context of colorectal cancer. *Biomaterials Science, 7*(8), 3386–3403. https://doi.org/10.1039/c9bm00393b

Castro, F., Pinto, M. L., Pereira, C. L., Serre, K., Barbosa, M. A., Vermaelen, K., et al. (2020). Chitosan/γ-PGA nanoparticles-based immunotherapy as adjuvant to radiotherapy in breast cancer. *Biomaterials, 257*, Article 120218. https://doi.org/10.1016/j.biomaterials.2020.120218

Chang, Z., Liu, F., Wang, L., Deng, M., Zhou, C., Sun, Q., et al. (2019). Near-infrared dyes, nanomaterials and proteins. *Chinese Chemical Letters, 30*(10), 1856–1882. https://doi.org/10.1016/j.cclet.2019.08.034

Christ, E., Wild, D., Forrer, F., Brändle, M., Sahli, R., Clerici, T., et al. (2009). Glucagon-like peptide-1 receptor imaging for localization of insulinomas. *Journal of Clinical*

Endocrinology and Metabolism, 94(11), 4398–4405. https://doi.org/10.1210/jc.2009-1082

Chung, J. H., Lee, J. S., & Lee, H. G. (2020). Resveratrol-loaded chitosan–γ-poly(glutamic acid) nanoparticles: Optimization, solubility, UV stability, and cellular antioxidant activity. *Colloids and Surfaces B: Biointerfaces, 186*, Article 110702. https://doi.org/10.1016/j.colsurfb.2019.110702

D'este, M., Eglin, D., & Alini, M (2014). A systematic analysis of DMTMM vs EDC/NHS for ligation of amines to Hyaluronan in water. *Carbohydrate Polymers, 108*, 239–246. https://doi.org/10.1016/j.carbpol.2014.02.070

Drucker, D. J. (2003). Glucagon-like peptides: Regulators of cell proliferation, differentiation, and apoptosis. *Molecular Endocrinology, 17*, 161–171. https://doi.org/10.1210/me.2002-0306

Elsabahy, M., Heo, G. S., Lim, S. M., Sun, G., & Wooley, K. L. (2015). Polymeric nanostructures for imaging and therapy. *Chemical Reviews, 115*(19), 10967–11011. https://doi.org/10.1021/acs.chemrev.5b00135

Gao, Y., & Wu, Y. (2022). Recent advances of chitosan-based nanoparticles for biomedical and biotechnological applications. *International Journal of Biological Macromolecules, 203*, 379–388. https://doi.org/10.1016/j.ijbiomac.2022.01.162

Geng, Y., Lin, D., Shao, L., Yan, F., & Ju, H. (2013). Cellular delivery of quantum dot-bound hybridization probe for detection of intracellular pre-microRNA using chitosan/poly(γ-glutamic acid) complex as a carrier. *PloS One, 8*(6), e65540. https://doi.org/10.1371/journal.pone.0065540

Hajdu, I., Bodnár, M., Filipcsei, G., Hartmann, J. F., Daróczi, L., Zrínyi, M., et al. (2008). Nanoparticles prepared by self-assembly of Chitosan and poly-γ-glutamic acid. *Colloid and Polymer Science, 286*(3), 343–350. https://doi.org/10.1007/s00396-007-1785-7

Hong, D. Y., Lee, J. S., & Lee, H. G. (2016). Chitosan/poly-γ-glutamic acid nanoparticles improve the solubility of lutein. *International Journal of Biological Macromolecules, 85*, 9–15. https://doi.org/10.1016/j.ijbiomac.2015.12.044

Jansen, T. J. P., van Lith, S. A. M., Boss, M., Brom, M., Joosten, L., Béhé, M., et al. (2019). Exendin-4 analogs in insulinoma theranostics. *Journal of Labelled Compounds and Radiopharmaceuticals, 62*(10), 656–672. https://doi.org/10.1002/jlcr.3750

Jirák, D., Kríz, J., Herynek, V., Andersson, B., Girman, P., Burian, M., et al. (2004). MRI of transplanted pancreatic islets. *Magnetic Resonance in Medicine, 52*(6), 1228–1233. https://doi.org/10.1002/mrm.20282

Keresztessy, Z., Bodnár, M., Ber, E., Hajdu, I., Zhang, M., Hartmann, J. F., et al. (2009). Self-assembling chitosan/poly-γ-glutamic acid nanoparticles for targeted drug delivery. *Colloid and Polymer Science, 287*(7), 759–765. https://doi.org/10.1007/s00396-009-2022-3

Khalil, I. R., Burns, A. T. H., Radecka, I., Kowalczuk, M., Khalaf, T., Adamus, G., et al. (2017). Bacterial-derived polymer poly-γ-glutamic acid (γ-PGA)-based micro/nanoparticles as a delivery system for antimicrobials and other biomedical applications. *International Journal of Molecular Sciences, 18*. https://doi.org/10.3390/ijms18020313

Kim, Hoe Suk, Tian, L., Lin, S., Cha, J. H., Jung, H. S., Park, K. S., et al. (2013). Magnetic labeling of pancreatic β-cells modulates the glucose- and insulin-induced phosphorylation of ERK1/2 and AKT. *Contrast Media and Molecular Imaging, 8*(1), 20–26. https://doi.org/10.1002/cmmi.1490

Kim, Hye Su, Lee, J. S., & Kim, M. Il (2020). Poly-γ-glutamic acid/chitosan hydrogel nanoparticles entrapping glucose oxidase and magnetic nanoparticles for glucose biosensing. *Journal of Nanoscience and Nanotechnology, 20*(9), 5333–5337. https://doi.org/10.1166/jnn.2020.17660

Körhegyi, Z., Rózsa, D., Hajdu, I., Bodnár, M., Kertész, I., Kerekes, K., et al. (2019). Synthesis of (68)Ga-labeled biopolymer-based nanoparticle imaging agents for positron-emission tomography. *Anticancer Research, 39*(5), 2415–2427. https://doi.org/10.21873/anticanres.13359

Körner, M., Christ, E., Wild, D., & Reubi, J. C. (2012). Glucagon-like peptide-1 receptor overexpression in cancer and its impact on clinical applications. *Frontiers in Endocrinology, 3*, 1–7. https://doi.org/10.3389/fendo.2012.00158. DEC.

Lebastchi, J., & Herold, K. C. (2012). Immunologic and metabolic biomarkers of β-cell destruction in the diagnosis of type 1 diabetes. *Cold Spring Harbor Perspectives in Medicine, 2*(6), 1–14. https://doi.org/10.1101/cshperspect.a007708

Li, J., Karunananthan, J., Pelham, B., & Kandeel, F. (2016). Imaging pancreatic islet cells by positron emission tomography. *World Journal of Radiology, 8*(9), 764–774. https://doi.org/10.4329/wjr.v8.i9.764

Lin, Y. H., Chung, C. K., Chen, C. T., Liang, H. F., Chen, S. C., & Sung, H. W. (2005). Preparation of nanoparticles composed of chitosan/poly-γ-glutamic acid and evaluation of their permeability through Caco-2 cells. *Biomacromolecules, 6*(2), 1104–1112. https://doi.org/10.1021/bm049312a

Lindheimer, F., Lindner, M. J., Oos, R., Honarpisheh, M., Zhang, Y., Lei, Y., et al. (2023). Non-invasive in vivo imaging of porcine islet xenografts in a preclinical model with [68Ga]Ga-exendin-4. *Frontiers in Nuclear Medicine, 3*. https://doi.org/10.3389/fnume.2023.1157480

Maddaloni, E., Bolli, G. B., Frier, B. M., Little, R. R., Leslie, R. D., Pozzilli, P., et al. (2022). C-peptide determination in the diagnosis of type of diabetes and its management: A clinical perspective. *Diabetes, Obesity & Metabolism, 24*(10), 1912–1926. https://doi.org/10.1111/dom.14785

Malhotra, A., Zhang, X., Turkson, J., & Santra, S. (2013). Buffer-stable chitosan-polyglutamic acid hybrid nanoparticles for biomedical applications. *Macromolecular Bioscience, 13*(5), 603–613. https://doi.org/10.1002/mabi.201200425

Montet, X., Lamprianou, S., Vinet, L., Meda, P., Fort, A., Wei, W., et al. (2013). Approaches for Imaging Pancreatic Islets: Recent Advances and Future Prospects BT - Islets of LangerhansM. S. Islam (Ed.), Approaches for Imaging Pancreatic Islets: Recent Advances and Future Prospects BT - Islets of Langerhans. *Advanced drug delivery reviews, 139*, 1–21. https://doi.org/10.1007/978-94-007-6884-0_39-2

Murakami, T., Fujimoto, H., & Inagaki, N. (2021). Non-invasive Beta-cell Imaging: Visualization, Quantification, and Beyond. *Frontiers in Endocrinology, 12*, Article 714348. https://doi.org/10.3389/fendo.2021.714348

Northrop, B. H., Frayne, S. H., & Choudhary, U. (2015). Thiol–maleimide "click" chemistry: Evaluating the influence of solvent, initiator, and thiol on the reaction mechanism, kinetics, and selectivity11Electronic supplementary information (ESI) available: Full experimental details and 1H NMR spectroscopic results of amine additions to NMM and of competition reactions between NMM, 7, and HT; full computational details regarding the calculation of nucleophilicity N indices and energetics of proton transfer from thiols 1 and 7 to DMF; plot of thiolate/Et3NH+ ion pair energies versus S···H distances; complete tables of all calculated rate constants; a kinetic plot of alkene conversion versus time for N-centered initiators in DMF; Cartesian coordinates of all stationary points reported in this manuscript; and the full author list for ref. 23. See 10.1039/c5py00168d *Polymer Chemistry, 6*(18), 3415–3430. https://doi.org/10.1039/c5py00168d.

Oishi, K., Miyamoto, Y., Saito, H., Murase, K., Ono, K., Sawada, M., et al. (2013). Vivo imaging of transplanted islets labeled with a novel cationic nanoparticle. *PLoS ONE, 8*(2), e57046. https://doi.org/10.1371/journal.pone.0057046

Reiner, T., Thurber, G., Gaglia, J., Vinegoni, C., Liew, C. W., Upadhyay, R., et al. (2011). Accurate measurement of pancreatic islet beta-cell mass using a second-generation fluorescent exendin-4 analog. *Proceedings of the National Academy of Sciences of the United States of America, 108*(31), 12815–12820. https://doi.org/10.1073/pnas.1109859108

Rossi, L., Kerekes, K., Kovács-Kocsi, J., Körhegyi, Z., Bodnár, M., Fazekas, E., et al. (2022a). Multivalent γ-PGA-Exendin-4 conjugates to target pancreatic β-Cells. *Chembiochem : a European Journal Of Chemical Biology.* , Article e202200196. https://doi.org/10.1002/CBIC.202200196

Rossi, L., Kerekes, K., Kovács-Kocsi, J., Körhegyi, Z., Bodnár, M., Fazekas, E., et al. (2022b). Multivalent γ-PGA-exendin-4 conjugates to target pancreatic β-Cells. *Chembiochem : a European Journal Of Chemical Biology*, (17), 23. https://doi.org/10.1002/cbic.202200196

Sidrak, M. M. A., De Feo, M. S., Corica, F., Gorica, J., Conte, M., Filippi, L., et al. (2023). Role of exendin-4 functional imaging in diagnosis of insulinoma: A systematic review. *Life (Basel, Switzerland), 13*(4). https://doi.org/10.3390/life13040989

Magli, Sofia, Giulia, B., Rossi, Giulia, Risi, Sabrina, Bertini, Cesare, Cosentino, Luca, et al. (2020). Design and synthesis of chitosan – gelatin hybrid hydrogels for 3D printable in vitro models. *Frontiers in Chemistry*. https://doi.org/10.3389/fchem.2020.00524

Vinet, L., Lamprianou, S., Babič, A., Lange, N., Thorel, F., Herrera, P. L., et al. (2015). Targeting GLP-1 receptors for repeated magnetic resonance imaging differentiates graded losses of pancreatic beta cells in mice. *Diabetologia, 58*(2), 304–312. https://doi.org/10.1007/s00125-014-3442-2

Wang, J., Liao, H., Ban, J., Li, S., Xiong, X., He, Q., et al. (2023). Multifunctional near-infrared Dye IR-817 encapsulated in albumin nanoparticles for enhanced imaging and photothermal therapy in melanoma. *International Journal of Nanomedicine, 18*, 4949–4967. https://doi.org/10.2147/IJN.S425013

Wang, P., Yoo, B., Yang, J., Zhang, X., Ross, A., Pantazopoulos, P., et al. (2014). GLP-1R-targeting magnetic nanoparticles for pancreatic islet imaging. *Diabetes, 63*(5), 1465–1474. https://doi.org/10.2337/db13-1543

Wang, W., Meng, Q., Li, Q., Liu, J., Zhou, M., Jin, Z., et al. (2020). Chitosan derivatives and their application in biomedicine. *International Journal of Molecular Sciences, 21*(2), 487. https://doi.org/10.3390/ijms21020487

Wei, W., Ehlerding, E. B., Lan, X., Luo, Q. Y., & Cai, W. (2019). Molecular imaging of β-cells: Diabetes and beyond. *Advanced Drug Delivery Reviews, 139*, 16–31. https://doi.org/10.1016/j.addr.2018.06.022

Wild, D., Martin, B., Christofori, G., Reubi, J. C., & Helmut, R. M. (2016). Promising ligand for glucagon-like peptide-1 (GLP-1) receptor targeting. *Journal of Nuclear Medicine, 40*, 2025–2034.

Wild, D., Wicki, A., Mansi, R., Béhé, M., Keil, B., Bernhardt, P., et al. (2010). Exendin-4-based radiopharmaceuticals for glucagonlike peptide-1 receptor PET/CT and SPECT/CT. *Journal of Nuclear Medicine*. https://doi.org/10.2967/jnumed.110.074914

Xu, H. L., Tong, M. Q., Wang, L. F., Chen, R., Li, X. Z., Sohawon, Y., et al. (2019). Thiolated γ-polyglutamic acid as a bioadhesive hydrogel-forming material: Evaluation of gelation, bioadhesive properties and sustained release of KGF in the repair of injured corneas. *Biomaterials Science, 7*(6), 2582–2599. https://doi.org/10.1039/c9bm00341j

Yu, M., Agarwal, D., Korutla, L., May, C. L., Wang, W., Griffith, N. N., et al. (2020). Islet transplantation in the subcutaneous space achieves long-term euglycaemia in preclinical models of type 1 diabetes. *Nature Metabolism, 2*(10), 1013–1020. https://doi.org/10.1038/s42255-020-0269-7

Zacharovová, K., Berková, Z., Jirák, D., Herynek, V., Vancová, M., Dovolilová, E., et al. (2012). Processing of superparamagnetic iron contrast agent ferucarbotran in transplanted pancreatic islets. *Contrast Media and Molecular Imaging, 7*(6), 485–493. https://doi.org/10.1002/cmmi.1477

Zhang, B., Yang, B., Zhai, C., Jiang, B., & Wu, Y. (2013). The role of exendin-4-conjugated superparamagnetic iron oxide nanoparticles in beta-cell-targeted MRI. *Biomaterials*. https://doi.org/10.1016/j.biomaterials.2013.04.021